Materials Today Bio 30 (2025) 101391

Contents lists available at ScienceDirect

Materials Today Bio

journal homepage: www.journals.elsevier.com/materials-today-bio

Structurally sophisticated 3D-printed PCL-fibrin hydrogel meniscal scaffold promotes in situ regeneration in the rabbit knee meniscus

Hebin Ma [a,b,c,d,1], Bowen Xie [d,1], Hongguang Chen [b,c,1], Lifang Hao [c], Haigang Jia [b], Dengjie Yu [a], Yuanbo Zhou [a,b,c], Puzhen Song [a,b], Yajing Li [e], Jing Liu [f], Kaitao Yu [g,*], Yantao Zhao [b,c,**], Yadong Zhang [b,h,***]

[a] Medical School of Chinese PLA, Beijing, 100853, PR China
[b] Department of Orthopedics, the Fourth Medical Center of PLA General Hospital, Beijing, 100048, PR China
[c] Beijing Engineering Research Center of Orthopedics Implants, Beijing, 100048, PR China
[d] Air Force Characteristic Medical Center, The Fifth School of Clinical Medicine, Anhui Medical University, Beijing, 100142, PR China
[e] Department of Respiratory and Critical Care Medicine, the Eighth Medical Center of Chinese PLA General Hospital, Beijing, 100091, PR China
[f] Department of Radiological, the Fourth Medical Center of PLA General Hospital, Beijing, 100048, PR China
[g] Department of Stomatology, the Fifth Medical Center of PLA General Hospital, Beijing, 100071, PR China
[h] Department of Orthopedics, the Fifth Medical Center of PLA General Hospital, Beijing, 100071, PR China

ARTICLE INFO

Keywords:
Meniscus
Tissue engineering
Hydrogel
Composite
Fibrin (Fib)
Polycaprolactone (PCL)

ABSTRACT

A meniscus injury is a common cartilage disease of the knee joint. Despite the availability of various methods for the treatment of meniscal injuries, the poor regenerative capacity of the meniscus often necessitates resection, leading to the accelerated progression of osteoarthritis. Advances in tissue engineering have introduced meniscal tissue engineering as a potential treatment option. In this study, we established the size of a standardized meniscal scaffold using knee Magnetic Resonance Imaging (MRI) data and created a precise Polycaprolactone (PCL) scaffold utilizing 3-Dimensional (3D) printing technology, which was then combined with Fibrin (Fib) hydrogel to form a PCL-Fib scaffold. The PCL scaffold offers superior biomechanical properties, while the Fib hydrogel creates a conducive microenvironment for cell growth, supporting chondrocyte proliferation and extracellular matrix (ECM) production. Physical and chemical characterization, biocompatibility testing, and in vivo animal experiments revealed the excellent biomechanical properties and biocompatibility of the scaffold, which enhanced in situ meniscal regeneration and reduced osteoarthritis progression. In conclusion, the integration of 3D printing technology and the Fib hydrogel provided a supportive microenvironment for chondrocyte proliferation and ECM secretion, facilitating the in situ regeneration and repair of the meniscal defect. This innovative approach presents a promising avenue for meniscal injury treatment and advances the clinical utilization of artificial meniscal grafts.

1. Introduction

The meniscus is a semilunar annular fibrocartilage located between the femoral condyle and the tibial plateau. It protects the articular cartilage from excessive strain and harm by redistributing loads, absorbing impacts, and contributing to the movement of the knee joint through its buffering capabilities [1–3]. The meniscus has a limited number of nerves and blood vessels, leading to delays in the detection and healing of injuries to this structure. Therefore, most symptomatic patients require partial or total meniscectomy, which accelerates joint aging and promotes the progression of osteoarthritis [4,5]. Several studies have shown that meniscal transplantation, particularly the allogeneic and synthetic menisci, is the most effective treatment option [6–9]. However, both meniscal scaffolds have shortcomings and cannot be widely used. Therefore, preparing a tissue-engineered meniscal scaffold with excellent mechanical properties, biocompatibility, and

* Corresponding author. Department of Stomatology, the Fifth Medical Center of PLA General Hospital, Beijing, 100071, PR China.
** Corresponding author. Department of Orthopedics, the Fourth Medical Center of PLA General Hospital, Beijing 100048, PR China.
*** Corresponding author. Department of Orthopedics, the Fifth Medical Center of PLA General Hospital, Beijing, 100071, PR China.
E-mail addresses: 13911890691@163.com (K. Yu), userzyt@qq.com (Y. Zhao), drzyd@126.com (Y. Zhang).
[1] These authors contributed equally to this work.

https://doi.org/10.1016/j.mtbio.2024.101391
Received 7 May 2024; Received in revised form 22 November 2024; Accepted 6 December 2024
Available online 11 December 2024

regeneration ability is of great significance for in situ meniscal regeneration.

With the rapid development of materials science in recent years, the tissue-engineered meniscus is expected to treat meniscal injuries effectively. Tissue engineering involves a combination of seeded cells, scaffold materials, and bioactive factors [10,11]. The scaffold material acts as an extracellular matrix (ECM), which bears the mechanical stress and provides a microenvironment for cell metabolism. Among the existing tissue engineering methods, 3-Dimensional (3D) printing technology and polymer synthetic degradable materials have been widely used for tissue regeneration and repair [12,13]. With 3D printing technology, the diameter inside the scaffold can be precisely designed, and the wire diameter and pore size can be controlled to achieve a bionic effect that can promote the regeneration and repair of tissues and organs [11,12,14]. Therefore, tissue-engineered menisci created using scaffold materials with excellent mechanical properties and biocompatibility and 3D printing technology show great potential in the treatment of meniscal injuries. Commonly used 3D printing materials in tissue engineering include polycaprolactone (PCL) [15,16], polyurethane (PU) [16], polyglycolic acid (PGA) [17] and polylactic acid (PLA) [18],.among others. Among them, PCL has low immunogenicity and biodegradability, and its degradation products can be metabolized through the tricarboxylic acid cycle without causing toxic side effects. It has been approved by the U.S. Food and Drug Administration and is widely used in regenerative medicine research [19,20]. Its melting temperature of 60 °C makes it easy to process and can simulate the morphology and controllable microstructure of collagen fibers inside the meniscus. In addition, PCL exhibits good mechanical properties and resistance to degradation.

Although PCL can support cell adhesion and proliferation, its hydrophobicity affects cell attachment to a certain extent, which may affect the therapeutic effect of the tissue-engineered meniscus [21]. Fibrin (Fib) is a natural biopolymer produced by crosslinking fibrinogen and thrombin. It is a long glycoprotein composed of a polypeptide chain containing three disulfide bonds [22,23]. Fib scaffolds are mainly divided into three forms: Fib hydrogel, Fib glue, and Fib microbeads [24]. The Fib hydrogel is made of purified fibrinogen, thrombin, and calcium salt. It is readily processable, extensively utilized, and regarded as one of the most promising biomaterials in the field of tissue engineering. On one hand, studies have shown that the molecular structure of the Fib hydrogel can improve the biomechanical properties of the material [25]. On the other hand, compared to other hydrogel materials, it can promote coagulation and neovascularization, significantly promoting the in situ regeneration and repair of the meniscus [22,26–28]. Ultimately, its excellent biocompatibility, it is widely used in the regeneration and repair of soft tissues, such as skin, blood vessels, muscles, and nerves [29,30]. Additionally, it has been widely used in clinical work as a carrier for autologous chondrocyte transplantation [31]. What's more, studies have demonstrated that Fib-based hydrogels are effective in treating meniscal injuries in animal models [32,33]. Although PCL and Fib hydrogel materials have been widely used in the field of tissue engineering, the PCL scaffold alone cannot provide an excellent microenvironment for tissue regeneration, and the poor mechanical properties of Fib alone cannot adapt to the stress in the knee joint. Thus, neither of these agents can meet the requirements of meniscal tissue engineering when used alone. There are few studies on the combined application of PCL material and Fib hydrogel scaffold for meniscal injury repair.

High-molecular degradable polymers can provide good biomechanical properties, Fib hydrogel can provide an excellent biocompatible microenvironment, thereby significantly improving the biocompatibility of the scaffold. The present study aimed to combine the 3D-printed PCL meniscal scaffold with Fib hydrogel to prepare a composite meniscal scaffold with tissue engineering properties. In addition, the physical and chemical properties and biocompatibility of the composite scaffold were evaluated, and its role in situ meniscal repair and articular cartilage protection in resection models were explored via animal experiments. The findings of this study will provide new ideas for the development and design of other tissue-engineered menisci and offer new treatment strategies for the clinical treatment of meniscal injuries. An overview of the study design is shown in Fig. 1.

2. Materials and methods

2.1. Preparation of the sophisticated PCL-Fib scaffold

2.1.1. Meniscus sizing and PCL scaffold preparation

A 7.0T Micromagnetic resonance imaging (MRI) (BioSpec70/30, Bruker, Germany) scan of the knee joint of male New Zealand Large White rabbits (bodyweight, 2.5–3 kg) was performed to obtain an anatomical model of the medial meniscus. The dimensional parameters were measured to determine the dimensions of the standardized meniscus. Based on the standardized meniscus model, digital modeling and layer slicing were performed using MP Bioprint software (MP Biotech, China) to generate 3D printable files. The file was imported to the MP Bioprint 3.0 bioprinter (LN435, Medprin Biotech, China), and the following printing parameters were set: temperature of the material cylinder, 130 °C; temperature of the nozzle, 150 °C; temperature of the thermostat table, 20 °C; ambient temperature, 20 °C; dispensing needle, G28; air pump pressure, 200 Kpa; speed of motion of the coordinate system, 3 pulses/ms, and screw rotation speed, 15 %. 3D meniscus scaffolds with a filament diameter of 150 μm and pore size of 250 μm were prepared using PCL (Mn = 80,000, P871874, Macklin, China) as the raw material (pre-experiment results).

2.1.2. Configuration of fibrinogen hydrogels and crosslinking agents

The Fib hydrogels were prepared by dissolving 1g of fibrinogen (20430ES08, Yeasen, China) in 10 ml of phosphate-buffered saline (PBS) (G4202, Servicebio, China) to prepare a 100 mg/mL fibrinogen solution. Subsequently, 2000 U of thrombin (20402ES05, Yeasen, China) was dissolved in 20 ml of 0.1 % BSA (36100ES25, Yeasen, China) solution to finally configure a 100 U/mL thrombin solution.

2.1.3. Crosslinking

The PCL scaffold was immersed in a fibrinogen hydrogel solution. After the formation of bubbles had ceased, the PCL-Fib composite scaffold was removed and immersed in thrombin solution for crosslinking at 37 °C for 4 h. The scaffold was precooled at −80 °C for 8 h, placed in a freeze dryer (FD8-3 aP, Gold-sim, Germany) for 24 h, and stored at 4 °C for spare use.

2.2. Sample characterization of the PCL-Fib scaffolds

2.2.1. Macroscopic and microstructural examinations

The general view of the scaffold was examined using a digital camera (Nikon, Japan), and the internal microstructure of the scaffold was photographed using a scanning electron microscope (SEM) (Apreo, ThermoFisher, USA). The cameras captured the surface and cross-sectional views of the scaffold.

2.2.2. Porosity and water absorption

The volume of the scaffold was calculated using the cylindrical volume formula and recorded as *V0*. A specific volume (recorded as *V1*) of absolute ethanol (Yili Fine Chemicals, China) was added to the graduated cylinder, and the scaffold was immersed. Utilize a Vacuum Dryer (DZF-6030, Shanghai Jinghong, China) to remove excess gas from the scaffold, ensuring it is completely filled with absolute ethanol. Finally, the scaffold filled with absolute ethanol was taken out and the volume of the ethanol remaining in the measuring cylinder was recorded (*V2*).

$$\text{The porosity of the scaffold} = (V1 - V2)/V0 \times 100\%$$

The weight of the scaffold was recorded and designated as *W0*. Then, the weight of the scaffold immersed in PBS solution was recorded after

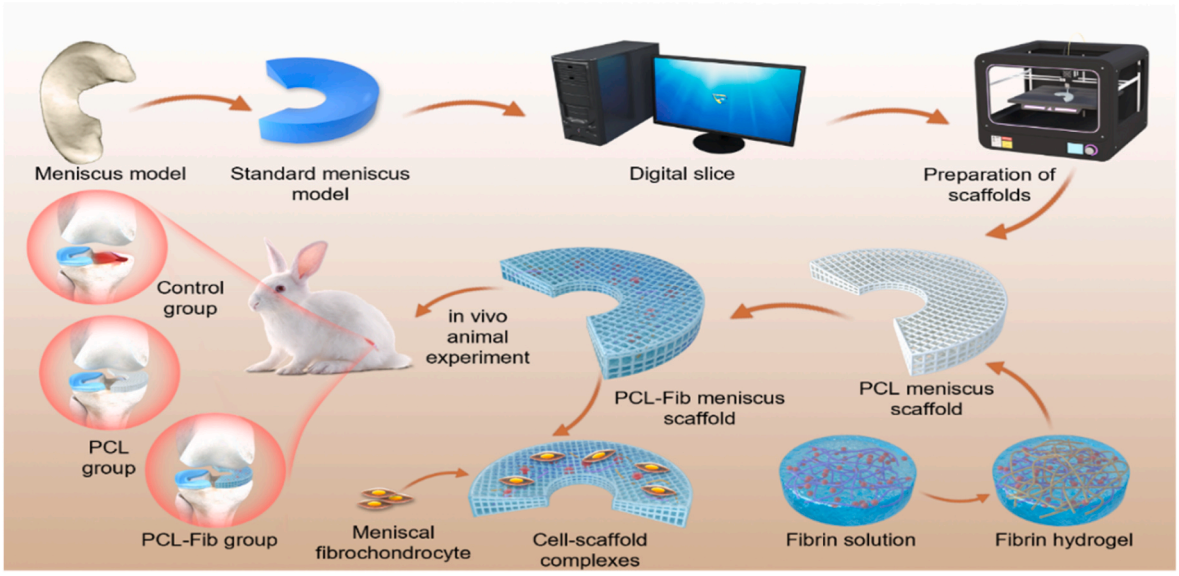

Fig. 1. Schematic diagram of the overall research design.

the formation of bubbles from the scaffold had ceased. A paper towel was used to wipe off the surface liquid (no apparent liquid outflow), and the scaffold was weighed again (recorded as *W1*).

The water absorption rate $= (W1 - W0)/W0 \times 100\%$

2.2.3. *In vitro degradation*

Two sets of scaffolds, both without MFCs involvement, were weighed (*W0*). Both sets were immersed in 0.5 U/ml proteinase XIV (P5147, Sigma, USA) [34] and incubated at 37 °C. On days 1, 3, 5, 7, and 14, the scaffolds were dried and weighed (recorded as *Wt*).

The scaffold degradation rate $= (W0 - Wt)/W0 \times 100\ \%$.

2.2.4. *Mechanical tests*

Compression testing was conducted on the PCL and PCL-Fib scaffolds using uniform specifications (compression: 9 mm diameter and 2 mm cylinder thickness; tensile: 75 mm outer length, 40 mm inner length, 10 mm outer width, 5 mm inner width, and 2 mm thickness of the long strip) and PBS infiltration. A biomechanical testing machine (CMT6104, Shandong Wanchen, China) was utilized for mechanical testing. All samples underwent unconfined compression testing at a strain rate of 5 mm/min and uniaxial tensile testing to failure at a rate of 20 mm/min. The compression and tensile moduli were determined based on the slopes of the linear parts of the strain–stress curves.

2.3. *Biological evaluation*

2.3.1. *Isolation and expansion of primary meniscal fibro chondrocytes (MFCs) from the rabbit meniscus*

The Institutional Animal Care and Use Committee of the Beijing Keyu approved all the animal experiment protocols for isolating the MFCs. Our approach to isolating, culturing, and passing seeded cells closely resembled that detailed in a prior publication [35]. MFCs were passaged after reaching confluence levels of 80 %–90 %, using 0.25 % trypsin (G4011, Servicebio, China) for digestion. Only cells within the range of P2–P5 were utilized in the study.

2.3.2. *Cytotoxicity test*

The toxicity of the scaffolds was evaluated using the Cell Counting Kit-8 (M4839, Abmole, USA). The scaffold extracts (0.2 g/ml) were prepared according to the ISO 10993-5 and 10993-12 protocols [36], filtered using a 0.22um needle filter and set aside. The MFCs (density, 5 $\times$ 10^3) were seeded individually in the wells of 96-well plates, and 100 μL of chondrocyte culture medium (90 % DMEM-F12; PYG004, Boster, China +10 % FBS; C2910, XP Biomed, China) was added to each well. On day 2, the cell culture in the plate was replaced with two groups of corresponding meniscal scaffold extract (chondrocyte medium was used as the control group). After day 5 of culture, 10 μL of CCK-8 solution was added to each well and incubated at 37 °C for 1 h. The absorbance was measured at 450 nm using Multiskan FC (1410101, ThermoFisher USA).

2.3.3. *Cell seeding*

The sterilized scaffolds (cobalt-60, 24 h) were moved to a clean bench; 100 μL of cell suspension (containing 5 $\times$ 10^6 cells/ml) was carefully dropped onto each scaffold, which was then placed in a cell incubator for 2 h to enhance cell adhesion. Subsequently, 1 ml of culture media was added, and the media was refreshed every 3 days.

2.3.4. *Morphology and attachment of MFCs on the scaffold*

The morphology of MFCs on both scaffolds was observed under a fluorescence microscope (IX-71, Olympus, Japan). After 3 days of incubation, the cell-scaffold complexes were washed three times with PBS for 5 min each and fixed with 4 % paraformaldehyde (G1101, Servicebio, China) for 30 min at RT. The cell membranes were broken for 20 min using 0.1 % Triton X-100 (T434386, Aladdin, China) solution, thus facilitating the entry of the staining agent, stained with F-actin (C2201S, Beyotime, China), and incubated at 37 °C for 1 h. Next, the MFCs were washed thrice with PBS, stained with DAPI (C1002, Beyotime, China) for 10 min, and washed twice. The cell growth was observed and photographed. In addition, SEM was used to observe the cell morphologies of the MFCs on the scaffold. The cell-scaffold complexes were washed thrice with PBS and fixed with glutaraldehyde (2.5 %; G6257, Sigma, USA) for 15 min. All specimens underwent dehydration via a succession of alcohol gradations and were dried at room temperature. The desiccated specimens were coated with a gold-palladium mixture and examined using an SEM at 1 KV.

2.3.5. *Cell viability assay*

The viability of MFCs on various scaffolds was assessed after 3 days of culture using the Live/Dead Assay kit (C2015M, Beyotime, China) and fluorescence microscopy. The cells were treated with 500 μL of a solution containing 1 mM Calcein-AM and 1 mM propidium iodide reagents and incubated at room temperature for 1 h. Excitation wavelengths of 488 and 568 nm were employed to visualize the live cells stained with

Calcein-AM (green fluorescence) and dead cells stained with propidium iodide (red fluorescence). Image J software (National Institutes of Health, USA) was utilized to analyze the images, and the cell viability rate was determined by the following formula: (number of live cells/total number of cells) × 100 %.

The viability of MFCs on different scaffolds was quantified using the Alamar Blue assay (40202ES80, Yeasen, China), with cells cultured in a dish serving as the positive control. After 1, 3, 5, 7 and 14 days of culture, 50 μL of Alamar Blue solution was added to the medium and incubated for 4 h at 37 °C. The optical density was measured at 570 nm using Multiskan FC.

2.3.6. Biocompatibility analysis of the scaffolds

The DNA, glycosaminoglycans (GAG), and hydroxyproline (HYP) levels in the cell-scaffold complexes were quantitatively analyzed after 3, 5, 7, and 14 days of incubation to determine the ability of MFCs to secrete cartilage matrix, as described in our previous study [37]. The cell-scaffold complexes underwent digestion with a preprepared solution (125 mg/mL of papain, 5 mM L-cysteine, 100 mM Na2HPO4, and 5 mM EDTA; pH 6.2) from Sigma, USA, at 60 °C for 16 h to estimate the DNA and GAG levels. The DNA content in the mixed solution was detected using a Qubit Flex fluorophore (Q33327, ThermoFisher, USA) according to the instructions of the DNA quantification kit (12640ES76, Yeasen, China). The GAG and hydroxyproline content in the cell-scaffold complexes was detected using the GAG Assay Kit (H480-1, Nanjingjiancheng, China) and the HYP Assay Kit(BC0255, Solarbio, China). Finally, the ability to secrete GAG and HYP per unit cell was analyzed based on the DNA content in each group.

2.3.7. Gene expression analysis in vitro

mRNA was initially isolated after lysis in Trizol (DP424, Tiangen, China) to analyze the gene expression on the cell-scaffold complexes using reverse transcription-polymerase chain reaction (RT-PCR), as described previously [3]. Subsequently, the mRNA levels were determined using a Nanodrop spectrophotometer (DS-500, YiPuyiqi, China). The extracted total RNA was reverse transcribed into cDNA utilizing the High-Capacity cDNA Reverse Transcription Kit (AG11728, Accurate Biology, China). Quantitative RT-PCR was conducted employing the SYBR Green PCR Master Mix (Q711-03, Vazyme Biotech, China) to assess specific gene expression (COL-I, COL-II, SOX 9, and Aggrecan) using an ABI Quant Studio 7 Flex Real-Time PCR System (4485701. Thermo Fisher, USA) according to the established protocols [38]. The RT-PCR protocol was as follows: 95 °C for 3 min, 95 °C for 10s, 60 °C for 30 s, and 40 cycles. GAPDH mRNA was used for internal reference. The target gene expression was normalized to that of the GAPDH mRNA using the ΔΔCt method for quantitative analysis. The list of primers used in this study is presented in Table 1.

2.3.8. Evaluation of the biocompatibility in vivo

Following approval from the Beijing Keyu Animal Breeding Centre, 12 Sprague Dawley (SD) rats were selected for the in vivo biocompatibility evaluations of the two groups of scaffolds. After anesthesia, the two groups of scaffolds were implanted separately into the rats' dorsal subcutaneous tissues, and the dorsal skin was sutured. Three rats were randomly sacrificed by euthanasia one week and one month after implantation. The material from the executed rats was collected, and Hematoxylin-Eosin (H&E) staining of the scaffolds was performed to observe the immune responses induced by the scaffolds in the surrounding skin after one week and one month) and evaluate the internal angiogenesis after one month.

Table 1
List of Primers used for the chondrogenic-related markers.

Gene	Sequence	
	Forward(5'-3')	Reverse(5'-3')
GADPH	CAAGAAGGTGGTGAAGCAGG	CACTGTTGAAGTCGCAGGAG
Aggrecan	GGAGGAGCAGGAGTTTGTCAA	TGTCCATCCGACCAGCGAAA
COL-1	GCCACCTGCCAGTCTTTACA	CCATCATCACCATCTCTGCCT
COL-2	CACGCTCAAGTCCCTCAACA	TCTATCCAGTAGTCACCGCTCT
SOX9	GCGGAGGAAGTCGGTGAAGAAT	AAGATGGCGTTGGGCGAGAT

2.4. In vivo implantation

2.4.1. Surgical procedure

The Beijing Keyu Animal Breeding Centre facilitated the utilization of New Zealand white rabbits in this research. The study was carried out in accordance with the guidelines outlined in the Guide for the Care and Use of Laboratory Animals (National Academy Press, National Institutes of Health Publication No. 85-23, Revised 1996). The experimental procedures were approved by the Institutional Animal Care and Use Committee of the Beijing Keyu (KY20220922006). New Zealand Large White rabbits weighing 2.5–3 kg were categorized into three groups prior to the operation: Control, PCL, and PCL-Fib.

During the surgical procedure, the rabbits were intravenously administered 10 mL of ethyl carbamate (0.2 g/mL) for anesthesia. Following disinfection and draping of the skin, a cut was made in the anteromedial parapatellar region to expose the medial meniscus by sectioning the medial collateral ligament. Subsequently, two surgical sutures were utilized and passed through the anterior and posterior corners of the meniscus. The sutures were passed through the syringe needle to the outside of the lateral knee fascia and secured with a knot for fixation. Finally, the knee was moved to evaluate the fixation of the brace. Different surgical methods were performed in the three groups. Total medial meniscectomy of the knee without implantation of the graft was performed in the control group; meniscectomy + PCL scaffold implantation was performed in the PCL scaffold group; and meniscectomy + PCL/Fib scaffold implantation was performed in the PCL/Fib group. The joint capsule was sealed, the medial collateral ligament was sutured, and the wound was closed after attaching the corners of the scaffold to the lateral knee fascia with sutures and knots. Postoperatively, all animals received prophylactic antibiotics with 10 mg/kg of penicillin for 3 days. Euthanasia was administered to all rabbits at 3 and 6 months following the surgery.

2.4.2. X-ray imaging and MRI

The femoral and tibiofibular diaphragms of the rabbit's affected limb were isolated, taking care not to open the articular cavity in the knee joint. The coronal and sagittal planes of the rabbit knee joint were examined using X-rays (GE Company, USA) and MRI 7.0T(BioSpec70/30, Bruker Company, Germany), respectively. According to the X-ray and MRI images, joint space of each time point, X-ray and MRI images, joint space, osteophytes, *neo-meniscus (it is the meniscus scaffold that was removed from the animals at the indicated times)*, and articular cartilage wear in each group through the Kellgren–Lawrence (K–L) score and Whole-Organ Magnetic Resonance Imaging Score (WORMS) [39,40] scoring system and other related osteoarthritis progression. The X-ray and MRI views were also evaluated blindly according to the K-L score system and WORMS scoring system by two independent trained researchers.

2.4.3. Morphologic observations

The adjacent ligaments and surrounding soft tissues were separated after the dissection of the knee joint. The femoral condyles, tibial plateau, and *neo-meniscus* were visually examined, and images were captured (Nikon Japan). The following formula was used to determine the rate of meniscus coverage: percentage of *neo-meniscus* coverage = area of meniscus/area of tibial plateau × 100 % [41].

2.4.4. Histological analysis

The *neo-meniscus* was fixed in 4 % paraformaldehyde for 48 h, followed by dehydration, embedding in paraffin, and staining with H&E,

Toluidine Blue (TB), and Safranin O/Fast greens (Saf O-Fg). Immunohistochemical staining was carried out to mark the type II collagen (IHC10589, Yaji Biological, China). Quantitative analysis of *the neo-meniscus* regeneration was conducted using the Pauli score [42]. The *neo-meniscus* were also evaluated blindly according to the Pauli score system by two independent trained researchers.

Samples from the femur and tibia were fixed in 4 % paraformaldehyde for 48 h and decalcified with Formate Decalcifying Solution (G1107, Servicebio, China) for 7 days to evaluate the articular surface. Following paraffin embedding, the samples were sectioned into 7-μm slices and stained with H&E, Saf O-Fg, and TB. The cartilage degeneration in the femoral condyle and tibial plateau was assessed using the Mankin score [43]. The femoral condyle and tibial plateau were also evaluated blindly according to the Mankin score system by two independent trained researchers.

2.5. Statistical analysis

The means ± standard deviations were used to express all the data in this study. Statistical analyses were conducted using the GraphPad Prism (ver. 8.0.3, GraphPad Software, USA). The data were checked for normality using the Shapiro–Wilk test, and significance tests were performed using analysis of variance or t-tests. A p-value of <0.05 indicated a statistically significant difference.

3. Results

3.1. Characterization of hybrid scaffolds

3.1.1. Macroscopic and microstructural features

The 3D-printed PCL scaffold had a uniform diameter and pore size with a similar anatomical appearance and internal structure to the natural meniscus tissue (Fig. 2A). The Fib hydrogel in the PCL-Fib scaffold was uniformly distributed within the pores of the scaffold,

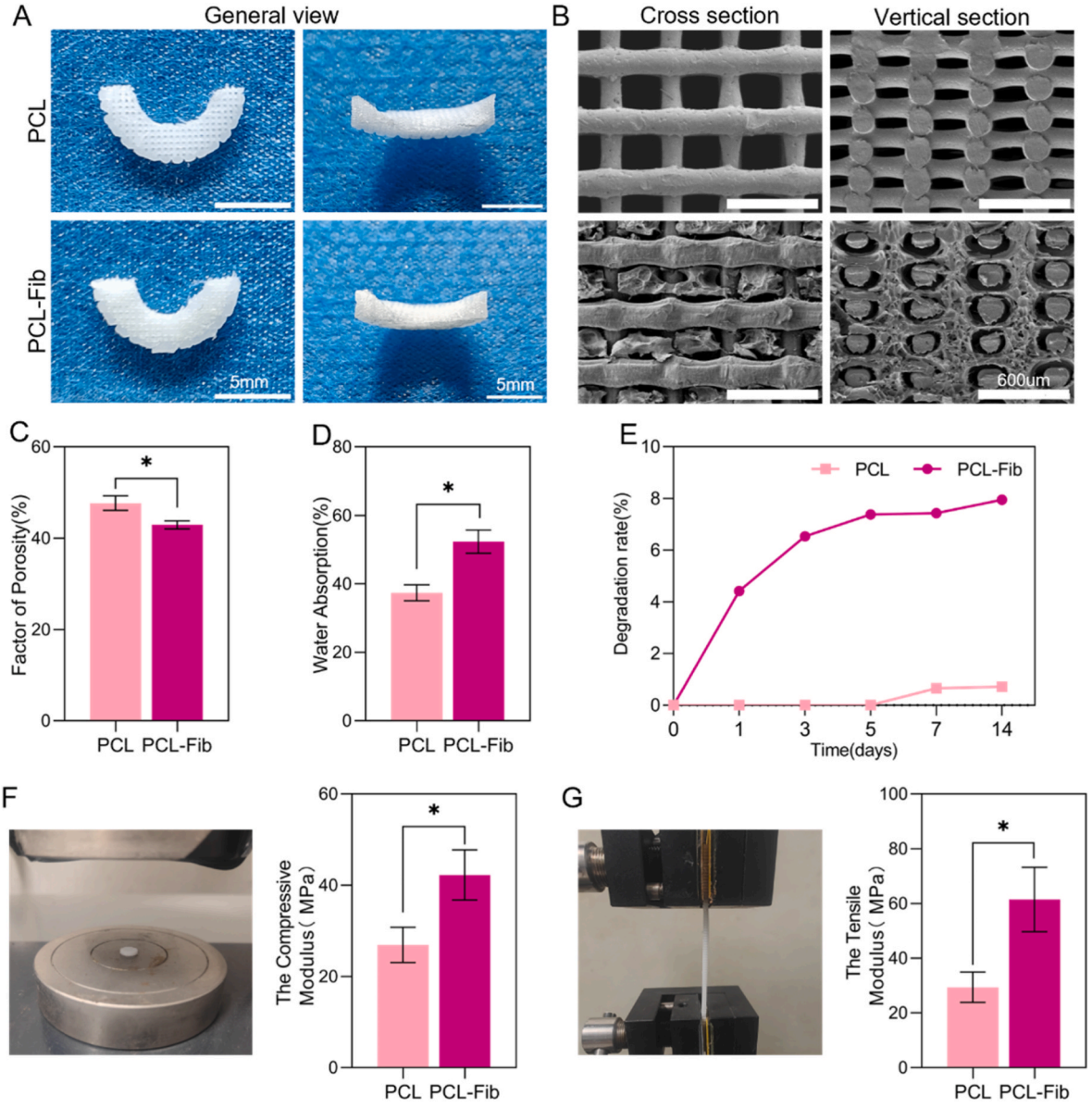

Fig. 2. Characterization of hybrid scaffolds. A) Macroscopic images. B) Microstructure of the scaffolds in cross and vertical section. C) Porosity of the scaffolds. D) Water absorption of the scaffolds. E) Degradation rate of the scaffolds. F) Compression modulus of the scaffolds in vitro. G) Tensile modulus of the scaffolds(n = 5, *p < 0.05).

and the composite effect between the two materials was good. Cross-sectional SEM showed a horizontal and vertical internal cross-structure of the PCL scaffold, and the thickness of the wire diameter was uniform (Fig. 2B).

Transverse-sectional images showed that the PCL scaffold was intersectional. The internal structure of the PCL-Fib scaffold was full of Fib hydrogel material, forming a porous structure.

3.1.2. Porosity and water absorption

As illustrated in Fig. 2C, the PCL scaffold exhibited a porosity rate of 47.68 ± 1.59 %, while the porosity of the PCL-Fib scaffold was 42.93 ± 0.88 %. As shown in Fig. 2D, the water absorption rate in the PCL group was 37.37 ± 2.35 %, whereas that in the PCL-Fib group was notably higher at 52.31 ± 3.38 %.

3.1.3. Degradation in vitro

As displayed in Fig. 2E, the overall degradation trend in the PCL scaffolds was slow and stable, and the degradation rate of the PCL scaffold at 14 days was 0.71 ± 0.99 %. However, due to the inherent properties of the hydrogel material, the degradation rate of the PCL-Fib scaffold was 7.38 ± 1.35 % during the first 5 days and 7.43 ± 1.43 % and 7.95 ± 1.56 % after 7 and 14 days, similar to the degradation trend in the PCL group.

3.1.4. Mechanical testing

Compressive and tensile moduli were determined by analyzing the

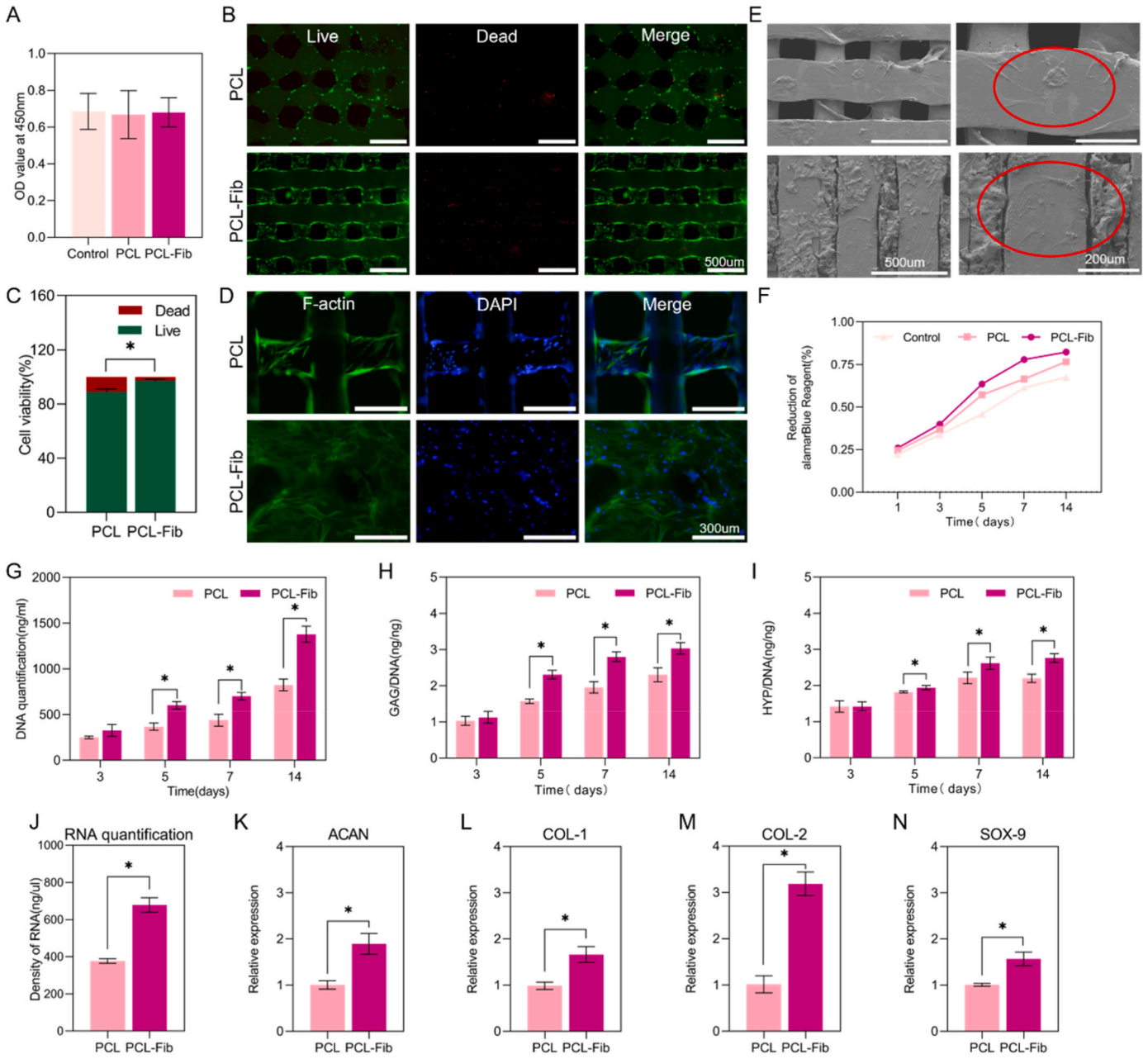

Fig. 3. Biocompatibility of MFCs in the scaffolds in vitro. A) CCK-8 assay of MFCs after 3 days of culturing with different scaffolds. B) Viability of MFCs was analyzed by Live/Dead staining 3 days after seeding on different scaffolds. C) Live/dead cell area ratio D) Morphology of MFCs was observed via F-actin/DAPI assay after 3 days of culturing with different scaffolds. E) Cell adhesion observed by SEM. F) Viability of MFCs in different groups was observed by alamarBlue assay. G) DNA content. H-I) GAG and HYP production in different scaffolds. J) mRNA content. K-N) Cartilage-specific gene expression of ACAN, COL-1, COL-2 and SOX-9 (n = 5, *p < 0.05).

slope of the linear portion of the stress-strain curve (Fig. 2G). The compression modulus in the PCL and PCL-Fib scaffolds were 26.91 ± 3.86 and 42.25 ± 5.47 MPa, respectively. The tensile modulus were 29.35 ± 5.54 and 61.45 ± 11.75 MPa in the PCL and PCL-Fib scaffolds, respectively. The compression and tensile moduli of the PCL-Fib scaffold were significantly higher than those of the PCL scaffold.

3.2. Biocompatibility analysis of the scaffolds

3.2.1. Cytotoxicity

In the CCK-8 experiment (Fig. 3A), no statistical differences in absorbance value were observed among the control, PCL, and PCL-Fib groups, indicating that neither the PCL nor the PCL-Fib group had obvious toxic and adverse side effects. After incubation on the scaffolds for 3 days, live/dead cell staining(Fig. 3B) showed that the MFCs were evenly distributed on the surfaces of the internal filament diameters of the PCL and the PCL-Fib scaffolds. Additionally, a notable increase in cell count was observed within the PCL-Fib scaffold compared to the PCL scaffold group. Furthermore, examination of the live/dead cell area ratio (Fig. 3C) revealed a significantly higher percentage of viable cells in the PCL-Fib scaffold group than in the PCL scaffold group. These results indicate favorable cellular compatibility in the PCL scaffold and PCL-Fib scaffold groups, with the incorporation of Fib hydrogel material notably enhancing the proliferation of MFCs.

3.2.2. Morphology of MFCs on the scaffold

After incubation on the scaffolds for 3 days, Actin-Tracker Green-488/DAPI staining was performed to observe the growth status and appearance of the cells in both scaffolds via fluorescence microscopy (Fig. 3D). The MFCs were successfully attached to the filament diameter of the PCL scaffold and showed good growth. The cells were uniformly distributed on the hydrogel material inside the PCL-Fib scaffold, and the number of MFCs was significantly higher than that in the PCL scaffold. In addition, SEM revealed that the chondrocytes were evenly distributed on the surface of the internal filament diameter of the PCL scaffold (Fig. 3E). The hydrogel material was evenly distributed in the interior of the PCL-Fib scaffold, and the number of cells was significantly higher than that in the PCL group, with a steady growth state. This finding indicated that the combination of hydrogel materials was conducive to cell migration and adhesion.

3.2.3. Cell viability

Following a 14-day incubation period in vitro, we evaluated the cellular metabolic function on the scaffold using Alamar Blue solution (Fig. 3F). The MFCs exhibited favorable proliferation on both types of scaffolds. Although no notable distinctions were observed among the three cell groups on days 1 and 3 of cultivation, a noticeable increase in metabolic activity was noted in the two scaffold groups compared to the control group after the fifth day of incubation. Additionally, the metabolic function in the PCL-Fib scaffold surpassed that in the PCL scaffold.

3.2.4. Biochemical content

According to the quantitative DNA results (Fig. 3G), the DNA content in both groups of scaffolds slowly increased with the extension of time during the culture process. However, on the 5th, 7th, and 14th day of culture, the DNA content in the PCL-Fib scaffold was significantly higher than that in the PCL scaffold. Thus, the PCL-Fib scaffold demonstrated enhanced MFC proliferation. The fibrocartilaginous matrix production was quantified by measuring the GAG and HYP levels, which were then normalized to the DNA content. Noteworthy increases in GAG and HYP secretion were observed from individual MFCs within the PCL-Fib scaffold compared to those in the PCL scaffold on days 5, 7, and 14 of in vitro culture (Fig. 3H and I), indicating that the PCL-Fib scaffold was significantly better than PCL scaffold in promoting ECM generation.

3.2.5. In vitro gene expression analysis

After 14 days of culture in vitro, the total mRNA content and the expression levels of related genes were quantitatively analyzed. The PCL-Fib scaffold could promote the increase in total mRNA in the MFCs (Fig. 3J). RT-PCR results showed (Fig. 3K–N) that the expression levels of COL1, COL2, SOX9, and ACAN in the MFCs in the PCL-Fib scaffold were significantly higher than those in the PCL scaffold.

3.2.6. In vivo biocompatibility

Results of the subcutaneous immune responses and new vessels in the SD rats are shown in Fig. 4A. In the case of the acute inflammatory response (1 week), a small number of inflammatory cells (Blue circles: Small lymphocyte; Pink circles:Neutrophil) were observed inside the PCL scaffold (8.46 ± 1.70); in contrast, the PCL-Fib scaffold (84.02 ± 4.16) was infiltrated with many inflammatory cells (Pink circles: Neutrophil). In the case of the subacute inflammatory response (1 month), a significant decrease in the number of inflammatory cells (Blue circles:Small lymphocyte; Green circles:Macrophage cell) was observed in the PCL scaffold (4.41 ± 1.79), with significant connective tissue formation at the edge of the scaffold and a few new vessels; however, in the PCL-Fib scaffold (26.17 ± 3.25), the number of inflammatory cells (Yellow circle:Large lymphocyte) decreased significantly, and a large number of new vessels were seen. The area of the new vessels was significantly higher than that in the PCL group (Fig. 4B–D). At 1 week and 1 month, the number of inflammatory cells in the PCL-Fib group was significantly increased compared to that in the PCL group. After 1 month, the area of new blood vessels in the PCL-Fib group(26.09 ± 0.99) showed a noticeable increase compared to that in the PCL group (4.32 ± 0.0.67). These findings indicate that the PCL-Fib scaffold can enhance the formation of blood vessels.

3.3. In vivo animal study

In order to investigate whether the meniscal scaffold could promote the regeneration of new meniscus, we established a rabbit medial meniscus defect model. Concurrently, two groups of meniscal scaffolds were implanted into the knee joints, and the regenerative effects on the neonatal meniscus and articular cartilage wear were analyzed using a combination of imaging, gross observation, and pathology (Fig. 5A). Intraoperative images of the rabbit knee meniscal scaffolds are shown in Fig. 5B.

3.3.1. Macroscopic evaluation

Macroscopic images taken 3 and 6 months after surgery (Fig. 5D) revealed the formation of a *neo-meniscus* in the PCL and PCL-Fib groups; alternatively, only minimal synovial hyperplasia was observed in the control group, indicating the absence of a *neo-meniscus*. The PCL-Fib group showed increased regeneration of the collagen fibers, and the *neo-meniscus* surface was smooth compared to that in the PCL group. After 6 months, both groups showed improvements in the area and shape of the *neo-meniscus* compared to that seen at 3 months. Image J software was used to calculate the proportion of neo-meniscus covering the tibial plateau in order to evaluate the *neo-meniscus* tissue (in the control group, the area of the synovium tissue was calculated). The area of the *neo-meniscus* in the PCL-Fib group was larger than those in the PCL and control groups (Fig. 5C).

Various degrees of articular cartilage wear were observed in this study. The joint wear in the PCL-Fib group was mild, whereas the PCL group presented with increased joint cartilage wear and significantly thinner articular cartilage; the control group showed significant cartilage wear and tear with significant osteoarthritis. The degree of cartilage surface degeneration gradually increased with time in each group.

3.3.2. Histological assessment

In the H&E-stained tissues, the formation of collagen fiber-like tissues and numerous elongated fibroblast-like cells was observed in the

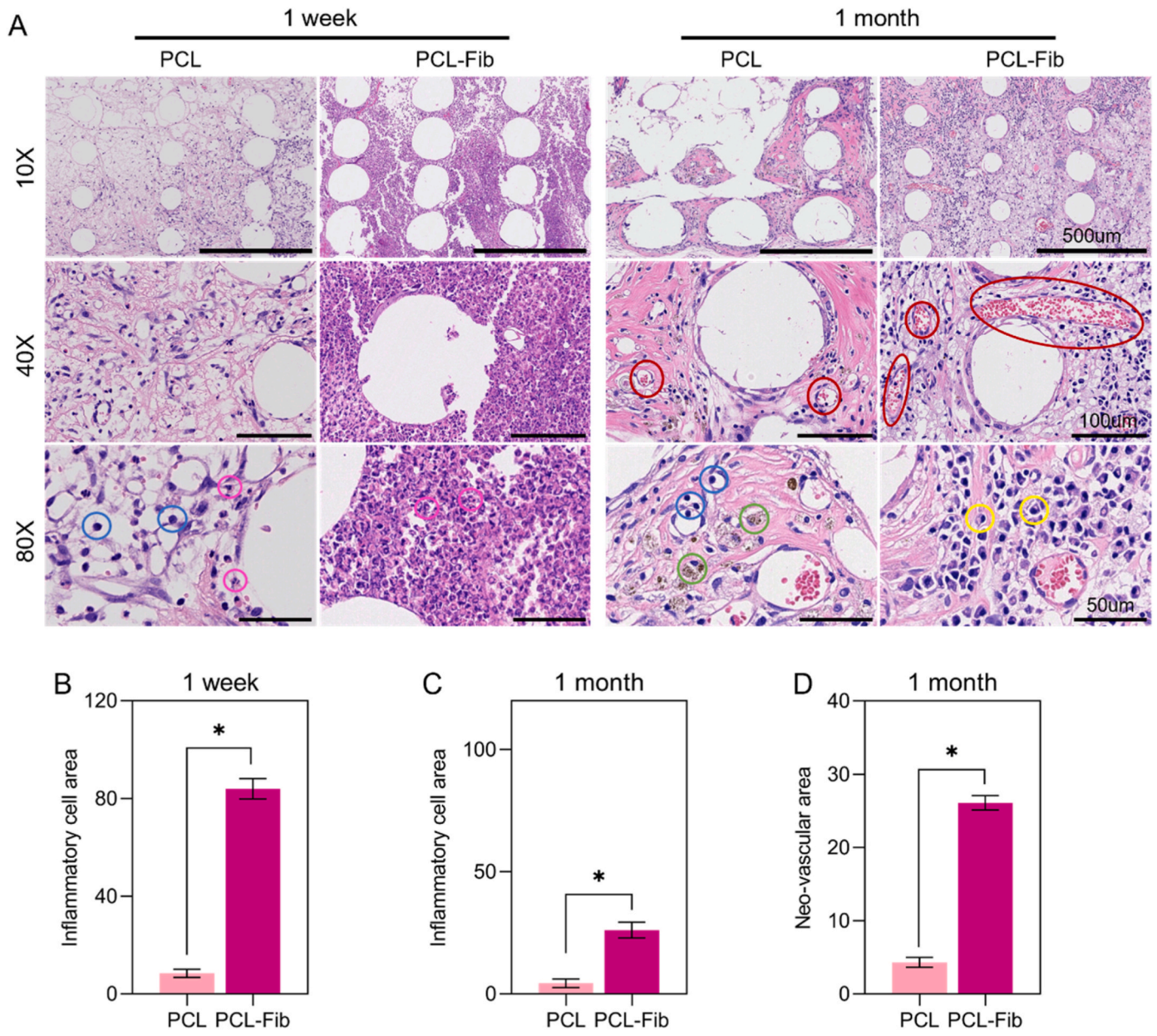

Fig. 4. Biocompatibility of MFCs in the scaffolds in vivo. A) Scaffolds HE staining results 1 week and 1 month after subcutaneous implantation. B–C) Ratio of inflammatory cell area 1 week and 1 month after surgery, respectively. D) Ratio of new-vessels area 1 month after surgery.

PCL-Fib group at 3 months after surgery, whereas only scattered chondroid cells were produced in the PCL group, and no obvious collagen fiber-like tissue formation was observed (Fig. 6A). At 6 months, the amount of collagen fiber-like tissues increased in both groups, and the PCL material was slightly degraded. The TB, Saf O-Fg, and type II collagen fiber staining showed positive expression for the *neo-meniscus* in both groups, which increased with time (Fig. 6B). The PCL-Fib group exhibited a significantly greater staining intensity than the PCL group. The Pauli scores for the *neo-meniscus* were notably higher in the PCL-Fib group than in the PCL group at each time point (Figs. 6C and 7D). Additionally, observation reveals that the remaining PCL area (the unstained portion) is clearly visible within the new meniscus. It has been conclusively shown that PCL does not completely degrade within 6 months.

Histological staining, including H&E, TB, and Saf O-Fg staining, was carried out on the femoral condyle and tibial plateau to examine the cartilage abrasion and assess the protective efficacy of the *neo-meniscus* tissue on the articular cartilage (Fig. 7A and B). The staining results revealed minimal harm to the articular cartilage in the PCL-Fib group, with only slight degeneration in the tibial plateau cartilage at 6 months post-implantation. On the contrary, the PCL group exhibited mild cartilage injury that worsened with time. The control group displayed signs of cartilage wear at 3 months, escalating to apparent damage at 6 months. The TB and Saf O-Fg staining results demonstrated positive expression of cartilage surfaces in all three groups, although the intensity of the staining decreased as time progressed. Notably, the staining intensity in the PCL-Fib group was significantly higher than that in the PCL group and control group. The Mankin's scores for the femoral condyle and tibial plateau cartilage in the PCL and PCL-Fib groups were superior to those in the control group.

3.3.3. *Image evaluation*

Based on the X-ray assessment of the health of the knee joint (Fig. 8A), the PCL-Fib group exhibited a normal joint space 3 months post-surgery. However, by the 6-month mark, the joint space had narrowed slightly, and the joint surface was slightly irregular. Conversely,

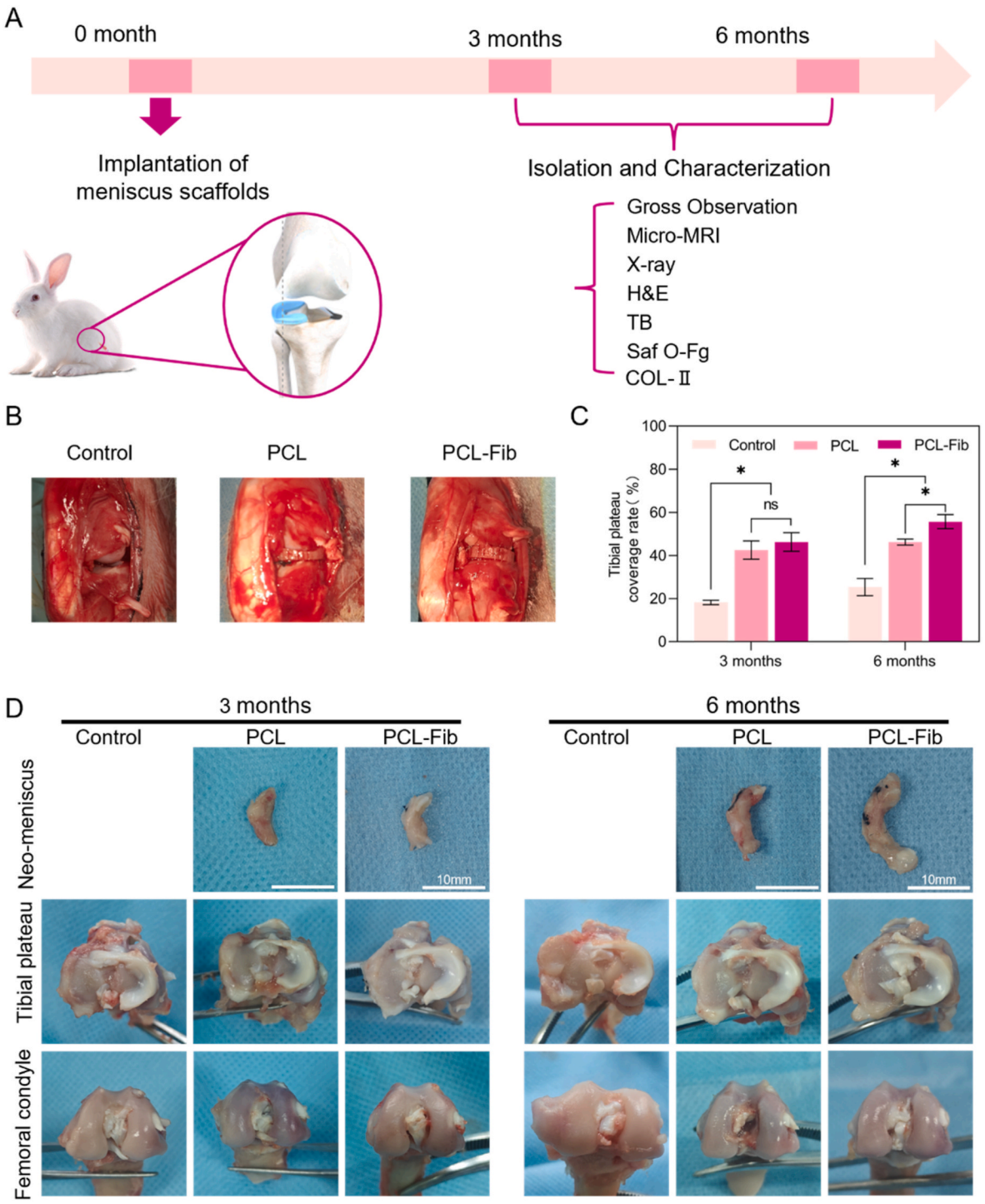

Fig. 5. Macroscopic observation of neo-meniscus in vivo. A) Stent implantation in each group of animals. B) Surgical photos of the three groups of animal experiments. C) Coverage of newborn meniscus. D) Gross views at 3 and 6 months after knee implantation.

the joint space in the PCL group had narrowed slightly and worsened at the 3-month evaluation. Additionally, indications of subchondral bone sclerosis and osteochondrosis were detected in this group at the 6-month evaluation. In contrast, the control group displayed a significantly narrowed joint space at 3 months, with obvious surface roughness; by 6 months, the joint space had further constricted, with significant bone growth, the development of osteophytes, and noticeable deformities. The K–L score data presented in Fig. 8B and C indicate notably lower (better) scores in the PCL-Fib and PCL groups than in the control group, with the PCL-Fib group achieving the lowest scores.

A knee MRI was performed to evaluate the wear of the *neo-meniscus* and articular cartilage (Fig. 8D). In the PCL-Fib group, the *neo-meniscus* was observed 3 months after surgery and grew over time. The articular cartilage surface was smooth, and no other obvious signs of osteoarthritis were noted. Likewise, the *neo-meniscus* was observed in the PCL group, but it was slightly smaller than in the PCL-Fib group, with a slight narrowing of the joint space, unevenness of the articular surface, synovitis, and cartilage wear. There was no *neo-meniscus* in the control groups, and cartilage wear and synovitis were observed. The WORMS scores (Fig. 8E and F) in the PCL and PCL-Fib groups were lower than

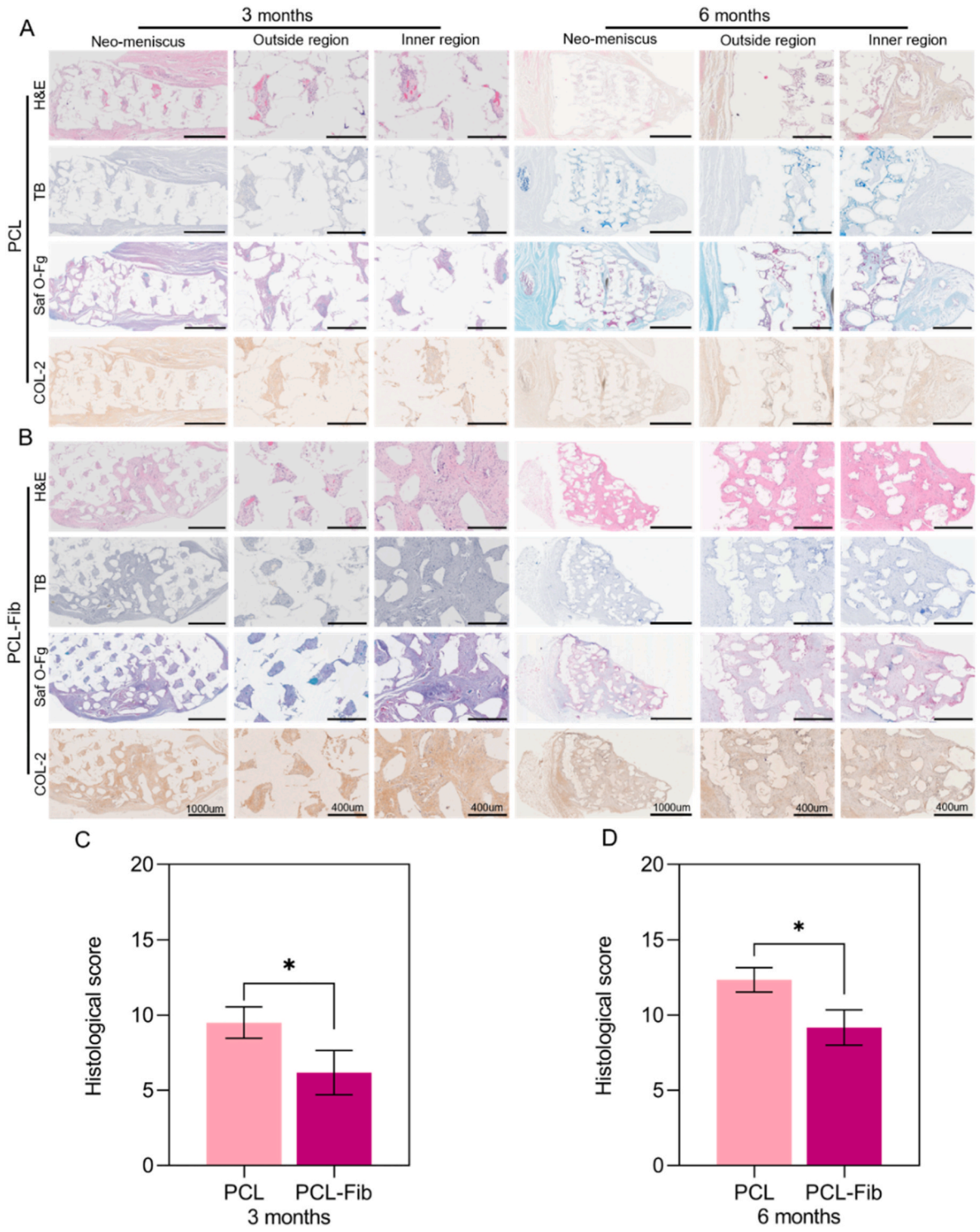

Fig. 6. Histological evaluation of the *neo-meniscus* in vivo. A-B) H&E, Toluidine Blue (TB), and Safranin O/Fast greens (Saf O-Fg) staining, immunohistochemical staining for COL-2. C-D) Histological scores of the *neo-meniscus* ($n = 6$,$^*p < 0.05$).

those the control group; at 6 months, the score in the PCL-Fib group was lower than that in the PCL group.

4. Discussion

With the continuous advancements in materials science and 3D printing technology, several attempts have been made to effectively apply the combination of the two fields to regenerate different tissues and organs [11,12]. Several studies on tissue engineering meniscus scaffolds have been conducted with favorable outcomes [34,44–46]. However, the exact therapeutic effect has not been achieved; moreover, using these techniques in clinical treatment is challenging. Therefore, in the current study, we optimized the internal structure of the meniscus scaffold through 3D printing technology, based on the characteristics of the meniscus, prepared the PCL meniscus scaffold (filament diameter, 150 μm; pore size, 250 μm) with a precise structure, and improved the biomechanical properties. This is a study to prepare a structurally precise meniscal composite scaffold with excellent cartilage repair

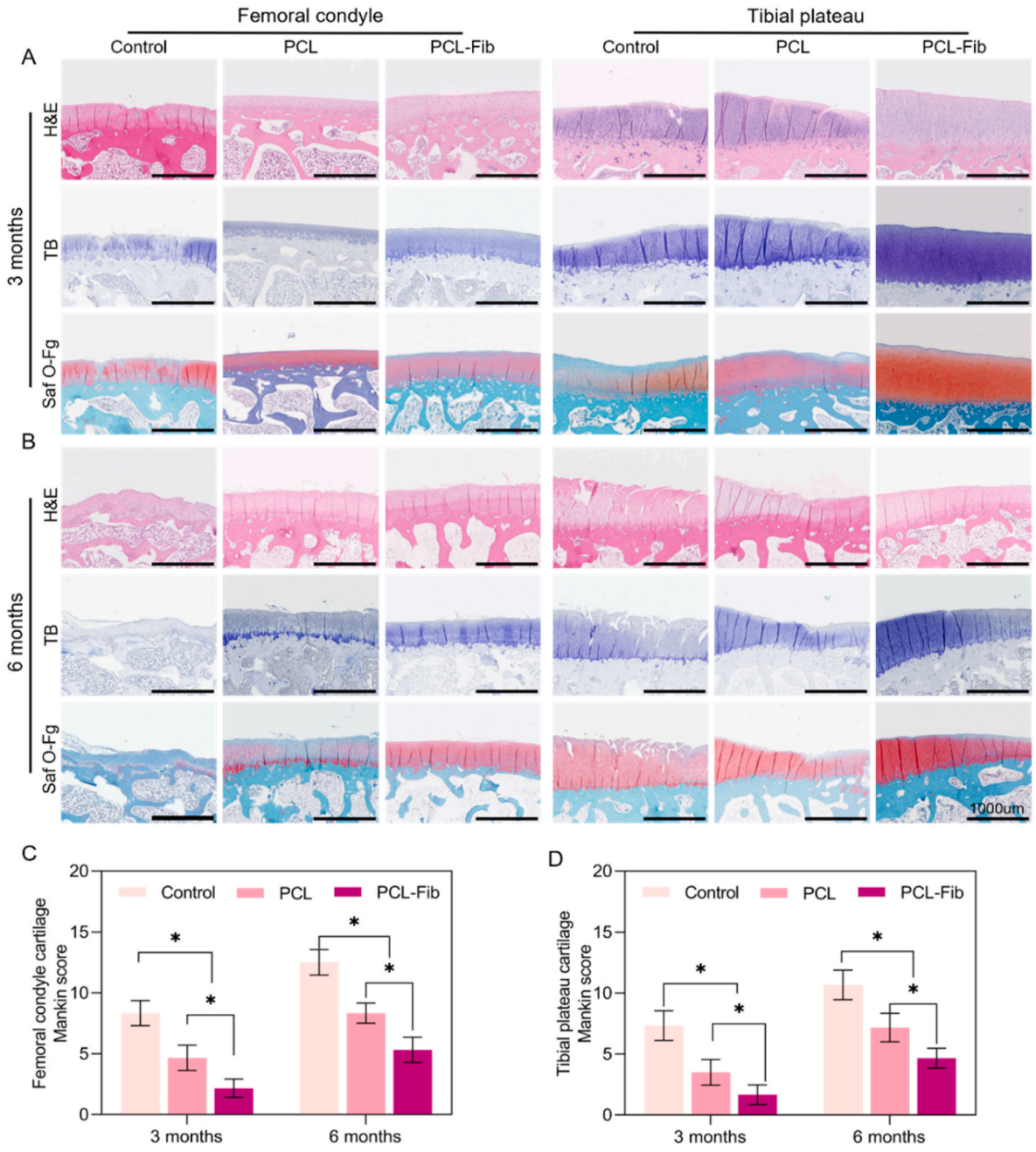

Fig. 7. Histological assessment of cartilage in vivo. A-B) Histological assessment (H&E, TB, and Saf O/Fg staining) of the femoral condyle and tibial plateau cartilage in different groups at 3 months and 6 months. C-D) Mankin scores of articular cartilage surfaces in the femoral condyle and tibial plateau ($n = 6$, $^*p < 0.05$).

properties by compositing PCL with Fib hydrogel. In addition to improving the biomechanical properties, it improves the regeneration effect of the meniscus defect and provides a feasible new method for treating meniscus injury by a tissue-engineered meniscus.

A PCL meniscus scaffold with precise structure was prepared using digital modeling and 3D printing technology, synthesized with fibrinogen solution, and crosslinked with thrombin and calcium salt to prepare the PCL-Fib meniscus scaffold. Studies have shown that the appropriate pore size for cells varies among the different tissues, and a size of 200–300 μm is the most suitable for promoting cell growth [47]. The diameter of fibers can affect the porosity, cell proliferation rate, and tensile modulus of the scaffolds [48]. The meniscus scaffolds prepared in the current study demonstrated excellent tensile and compressive moduli compared to other meniscus scaffolds of varying diameters and porosities [34,49]. The scaffold in the current study met the criteria for the compressive (1.52 ± 0.59 MPa) [50] and tensile (105 ± 58 MPa) moduli of the natural meniscus [51]. The biomechanical properties of the PCL-Fib scaffold were significantly better than those of the PCL scaffold, indicating that Fib hydrogel could enhance the biomechanical properties of the scaffold. The mechanical properties of the PCL-Fib scaffold were similar to those of the natural meniscus. The PCL-Fib scaffold had higher water absorption and lower porosity due to the combination of the hydrogel materials. Furthermore, the PCL-Fib scaffold had a rich pore structure, which could increase the adhesion area of cells, promote the information exchange between cells, and facilitate the metabolism of waste and the exchange of nutrients. The PCL scaffold demonstrated good biodegradation resistance from the beginning to the end. The faster degradation rate of the PCL-Fib scaffold within the first 5 days may be related to the intrinsic properties of Fib hydrogel materials; the degradation trend after that was the same as that of the PCL scaffold.

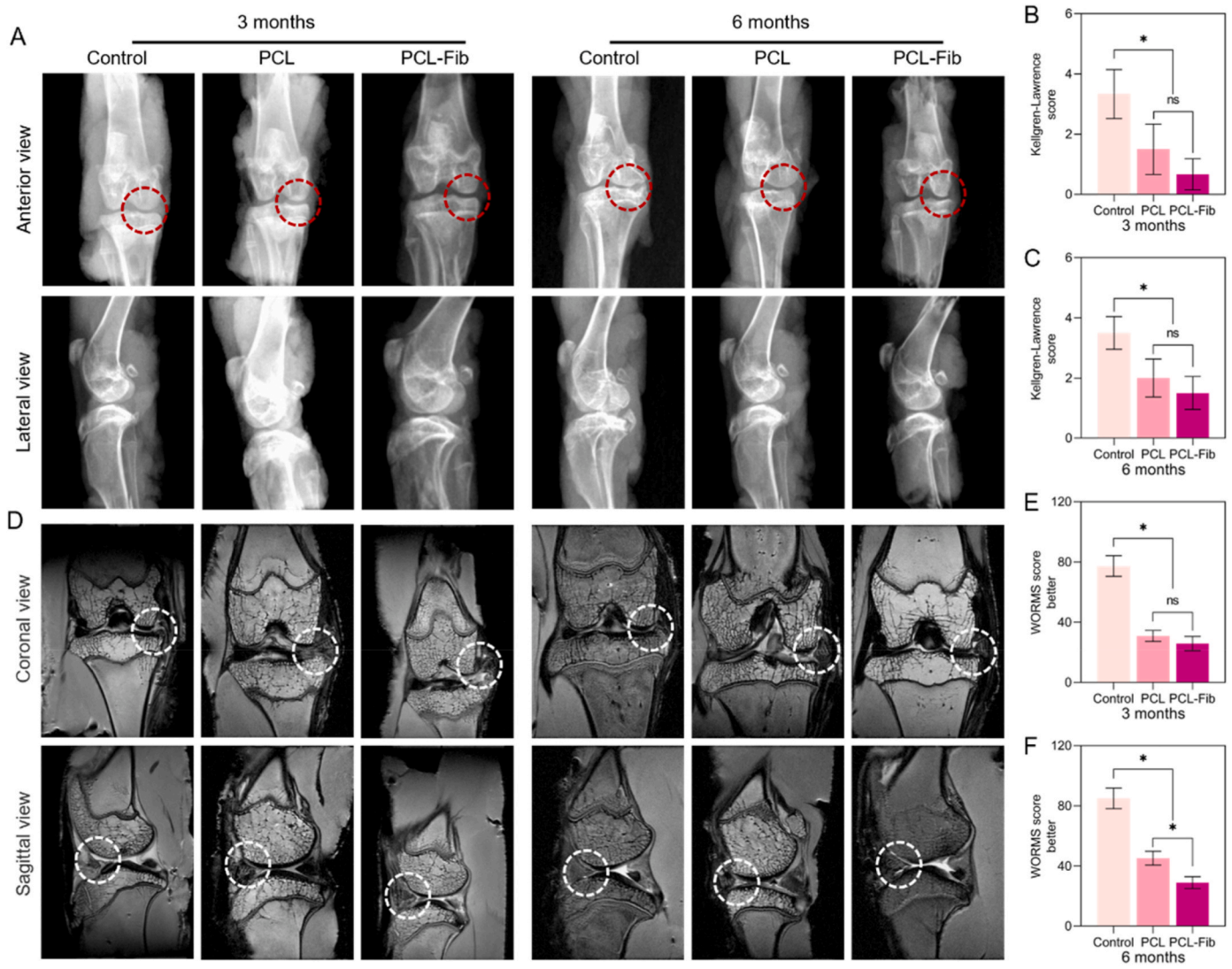

Fig. 8. Image evaluation. A) X-ray images of rabbit knee joints. B-C) K-L scores for X-ray. D) MRI images of rabbit knee joints. E-F) WORMS scores for MRI ($n = 6$,*$p < 0.05$).

The CCK-8 test is one of the commonly used methods to detect the biosafety of materials. The PCL-Fib and PCL scaffolds demonstrated good biosafety in the present study. Alamar Blue is an indicator of the oxidation–reduction reaction that produces absorbance changes and fluorescence signals based on the metabolic activity of cells. The advantage of this reagent is that it is nontoxic and harmless to cells and can continuously detect the metabolic activity of chondrocytes in the same sample. The cell activity in the PCL-Fib group was significantly stronger than those in the PCL and control groups. Live/dead staining experiments showed that the survival rates of cells on scaffolds in the PCL-Fib group were significantly higher than those in the PCL group, indicating that the Fib hydrogel material could promote the proliferation of chondrocytes. Cell staining and SEM were used to observe the adhesion and appearance of cells, respectively. The cells attached well to the PCL and PCL-Fib scaffolds, with a significantly higher number adhered to the PCL-Fib scaffold. As reported in a previous study [27], the Fib hydrogel can promote cell adhesion, proliferation, and migration.

The DNA content on the PCL-Fib scaffolds was higher than that in the PCL group, suggesting a greater number of cells in the PCL-Fib scaffolds, potentially due to the Fib hydrogel's ability to promote cell adhesion and provide a larger surface area for growth. The ECM in the meniscus is primarily composed of collagen and GAG [52,53]. The content of HYP comprises approximately 13 % of collagen. Therefore, we evaluated the ability of chondrocytes on the scaffolds to secrete ECM by measuring the content of HYP and GAG, thereby assessing their contribution to meniscal regeneration. To more accurately assess the ability of individual chondrocytes to secrete HYP and GAG, we normalized these values based on the DNA content. The graphs (Fig. 3H and I) clearly demonstrate that the ability of individual cells to secrete both HYP and GAG gradually increased during the first 7 days of culture, with the PCL-Fib group exhibiting a significantly greater capacity than the PCL group. The ability of individual cells to secrete HYP and GAG showed minimal change on day 14 of culture compared to day 7. This may be attributed to the gradual depletion of nutrients available to individual cells as cell density increased while nutrient content remained constant; concurrently, the capacity for nutrient exchange and waste removal may have approached its peak as cell proliferation occurred. Then, we assessed the RNA content and chondrogenic gene expression within the cell-scaffold complex. The RNA content in the PCL-Fib group was significantly higher than that in the PCL group, corroborating the observed differences in DNA content. PCR results further indicated that the expression levels of ACAN, SOX-9, COL-1, and COL-2 cartilage--forming genes were higher in the PCL-Fib group than in the PCL group. This finding further confirmed the reliability of the observed differences in the ability of chondrocytes to secrete ECM on the scaffolds between the two groups. The reasons for the above biochemical analysis results

were confirmed at the gene level. Similar to the findings of other studies [25,54–56], the Fib hydrogel promoted cell adhesion and ECM production in the current study.

Subsequently, the scaffold was subcutaneously implanted in rats to evaluate the immunogenicity of the scaffold and its ability to promote angiogenesis. After consulting relevant bibliographic [57–60], we determined that acute inflammation lasts only a few days to a month and is characterized by exudative lesions, primarily dominated by neutrophil infiltration. In contrast, chronic inflammation persists for extended periods, often months to years, and is typically characterized by a proliferative response, with infiltration of inflammatory cells mainly consisting of macrophage cell and lymphocyte cell. At the same time, it can be concluded from HE staining that 1 week after surgery, the inflammatory cells inside the PCL-Fib group are mainly neutrophil (Pink circles), the inflammatory cells in the PCL group are mainly small lymphocyte (Blue circles) and neutrophil; 1 month after surgery, the inflammatory cells inside the PCL-Fib group are mainly large lymphocyte (Yellow circle). The inflammatory cells in the PCL group are mainly small lymphocytes and macrophage cell (Green circles). From this, the types of inflammatory cells can be identified and the process of inflammation can be judged. Quantitative analysis revealed that, regardless of whether the observation period was one week or one month, the cell area of inflammation-related cells in the PCL group was significantly lower than that in the PCL-Fib group, indicating that the PCL group exhibited reduced immunogenicity.

However, as illustrated in Fig. 4A, at the one-month mark, the area of new blood vessels (Red circles in Fig. 4A) in the scaffold of the PCL-Fib group was significantly greater than that in the PCL group. This finding suggests that the PCL-Fib group effectively promotes vascular regeneration, with potential implications for enhancing angiogenesis and facilitating meniscus regeneration. Additionally, research by Liang Zhao et al. [61]. demonstrated that the application of PCL composite Fib materials in vascular tissue engineering can promote blood vessel regeneration. Similarly, Sebastian Freeman et al. [62]. utilized Fib to fabricate small-diameter blood vessels, demonstrating their potential to serve as equivalent blood vessel transplants to meet diverse patient needs. Collectively, these findings underscore the widespread applicability of Fib in vascular tissue engineering and its potential to enhance blood vessel formation. Furthermore, one of the primary challenges in meniscal regeneration and repair is the scarcity of blood vessels. This observation further supports the notion that PCL and Fib composites possess superior angiogenic capabilities. The results of this study corroborate this hypothesis and validate the efficacy of the experimental approach. Ultimately, it was established that the PCL-Fib scaffold can facilitate the formation of new blood vessels, thereby addressing the issue of vascular deficiency and effectively promoting the in situ regeneration of the meniscus, as reported previously [22,26,27].

A tissue-engineered meniscus scaffold was inserted into the medial meniscus of the knee joint, and the impact of the scaffold on in situ meniscus restoration and articular cartilage wear was examined in a rabbit model with a medial meniscus defect. The ability of the scaffold to delay the progression of osteoarthritis in meniscus defects was affirmed in this study. In vivo investigations indicated that the PCL and PCL-Fib scaffolds could stimulate meniscus regrowth despite notable distinctions in the dimensions, configurations, and histological compositions of the *neo-meniscus* in each treatment group. The formation of a *neo-meniscus* covering the tibial plateau was clearly visible in the PCL and PCL-Fib groups. This outcome may be attributed to the limitation of the pore structure of the PCL scaffold, which only offers structural support for tissue expansion but lacks an ideal microenvironment for cellular proliferation [63]. Moreover, the quality of the *neo-meniscus* in the PCL-Fib group exceeded that of the PCL group in terms of the histological makeup and overall impact. These findings emphasize the role of Fib hydrogel in situ meniscal regeneration. Previous studies have reported better biocompatibility of hydrogel materials to promote ECM production and maturation and remodeling of meniscal tissue [25,64,65]. In the control group, only regeneration of synovial tissue was observed, indicating that the meniscus does not regenerate effectively without intervention. The PCL-Fib scaffold effectively prevented cartilage degeneration and delayed the progression of osteoarthritis in the *neo-meniscus* compared to the PCL scaffold, which was consistent with the results of the histological analysis of the nascent meniscus.

The meniscus contributes to redistributing the loads and absorbing shocks to protect the articular cartilage from overload and damage, thereby acting as a cushion during knee movements [1–3]. Therefore, the volume of the meniscus significantly affects cartilage protection and joint wear [3,66,67]. A smaller meniscus increases the pressure on the articular cartilage and accelerates the progression of articular cartilage damage and osteoarthritis. Thus, in the control group, the absence of a meniscus and the increased load on the knee increased the severity of the articular cartilage damage.

While this study demonstrated promising therapeutic outcomes, it is important to acknowledge certain limitations. First, we did not evaluate the effect of different concentrations of Fib hydrogels on MFCs by referring to their fibrinogen concentrations because Fib hydrogels are used for cartilage repair. Second, only the biomechanical properties of the scaffolds were examined prior to in vitro testing. Therefore, the experiment is still in the preliminary stage, and there is still a long way to go before its clinical application. In the future, we aim to focus on the bionic design of the meniscus scaffold. The bionic design of the internal structure of the scaffold is conducive to the directional regeneration of new tissues and the improvement of the biomechanical properties of the scaffold. Additionally, seed cells and bioactive factors will be utilized comprehensively to enhance the characteristics of Fib drug delivery and cell compatibility. This approach aims to develop more effective tissue engineering scaffolds for meniscal regeneration and to further improve the regeneration effects of meniscus scaffolds.

5. Conclusions

In this study, 3D printing technology was used to develop a PCL meniscus scaffold with a precise structure. Fib hydrogel material was combined with the scaffold to prepare the PCL-Fib scaffold, which promoted the proliferation of chondrocytes, production of ECM in vitro, and in situ regeneration and repair of meniscus tissue; additionally, it delayed the wear of the articular cartilage in the meniscectomy model. The new meniscus scaffold structure and composite meniscus scheme introduced in this study can effectively improve the repair effect of the meniscus scaffold compared to the traditional meniscus tissue engineering method. Therefore, the PCL-Fib scaffold designed and prepared in this study has great clinical application potential in meniscus tissue engineering.

CRediT authorship contribution statement

Hebin Ma: Writing – original draft, Software, Methodology, Formal analysis, Data curation. **Bowen Xie:** Writing – review & editing, Project administration, Methodology, Formal analysis. **Hongguang Chen:** Project administration, Methodology, Formal analysis. **Lifang Hao:** Writing – review & editing. **Haigang Jia:** Visualization, Validation. **Dengjie Yu:** Visualization, Validation. **Yuanbo Zhou:** Writing – review & editing. **Puzhen Song:** Writing – review & editing. **Yajing Li:** Visualization, Validation. **Jing Liu:** Visualization, Validation. **Kaitao Yu:** Investigation, Conceptualization. **Yantao Zhao:** Investigation, Conceptualization. **Yadong Zhang:** Supervision, Funding acquisition, Conceptualization.

Declaration of competing interest

There is no conflict of interest regarding the publication of this article.

Acknowledgements

This work was supported by the National Natural Science Foundation of China (82072451), the Research and Translational Application of Clinical Characteristic Diagnosis and Treatment Techniques in the Capital (Z221100007422014) and the Natural Science Foundation of Beijing (7202199).

Appendix A. Supplementary data

Supplementary data to this article can be found online at https://doi.org/10.1016/j.mtbio.2024.101391.

Data availability

Data will be made available on request.

References

[1] P.S. Walker, M.J. Erkman, The role of the menisci in force transmission across the knee, Clin. Orthop. Relat. Res. 109 (1975) 184–192, https://doi.org/10.1097/00003086-197506000-00027.
[2] P.S. Walker, S. Arno, C. Bell, G. Salvadore, I. Borukhov, C. Oh, Function of the medial meniscus in force transmission and stability, J. Biomech. 48 (8) (2015) 1383–1388, https://doi.org/10.1016/j.jbiomech.2015.02.055.
[3] S. Gao, M. Chen, P. Wang, Y. Li, Z. Yuan, W. Guo, Z. Zhang, X. Zhang, X. Jing, X. Li, S. Liu, X. Sui, T. Xi, Q. Guo, An electrospun fiber reinforced scaffold promotes total meniscus regeneration in rabbit meniscectomy model, Acta Biomater. 73 (2018) 127–140, https://doi.org/10.1016/j.actbio.2018.04.012.
[4] J.N. Katz, R.H. Brophy, C.E. Chaisson, L. de Chaves, B.J. Cole, D.L. Dahm, L. A. Donnell-Fink, A. Guermazi, A.K. Haas, M.H. Jones, B.A. Levy, L.A. Mandl, S. D. Martin, R.G. Marx, A. Miniaci, M.J. Matava, J. Palmisano, E.K. Reinke, B. E. Richardson, B.N. Rome, C.E. Safran-Norton, D.J. Skoniecki, D.H. Solomon, M. V. Smith, K.P. Spindler, M.J. Stuart, J. Wright, R.W. Wright, E. Losina, Surgery versus physical therapy for a meniscal tear and osteoarthritis, N. Engl. J. Med. 368 (18) (2013) 1675–1684, https://doi.org/10.1056/NEJMoa1301408.
[5] J. Pak, J.H. Lee, K.S. Park, J.H. Jeon, S.H. Lee, Potential use of mesenchymal stem cells in human meniscal repair: current insights, Open Access J. Sports Med. 8 (2017) 33–38, https://doi.org/10.2147/oajsm.S113018.
[6] P.E. Gelber, A. Isart, J.I. Erquicia, X. Pelfort, M. Tey-Pons, J.C. Monllau, Partial meniscus substitution with a polyurethane scaffold does not improve outcome after an open-wedge high tibial osteotomy, Knee Surg. Sports Traumatol. Arthrosc. 23 (1) (2015) 334–339, https://doi.org/10.1007/s00167-014-3206-z.
[7] Z.Z. Zhang, S.J. Wang, J.Y. Zhang, W.B. Jiang, A.B. Huang, Y.S. Qi, J.X. Ding, X. S. Chen, D. Jiang, J.K. Yu, 3D-Printed poly(ε-caprolactone) scaffold augmented with mesenchymal stem cells for total meniscal substitution: a 12- and 24-week animal study in a rabbit model, Am. J. Sports Med. 45 (7) (2017) 1497–1511, https://doi.org/10.1177/0363546517691513.
[8] D. Jiang, Y.F. Ao, X. Gong, Y.J. Wang, Z.Z. Zheng, J.K. Yu, Comparative study on immediate versus delayed meniscus allograft transplantation: 4- to 6-year follow-up, Am. J. Sports Med. 42 (10) (2014) 2329–2337, https://doi.org/10.1177/0363546514541653.
[9] B. Bilgen, C.T. Jayasuriya, B.D. Owens, Current concepts in meniscus tissue engineering and repair, Adv. Healthcare Mater. 7 (11) (2018) e1701407, https://doi.org/10.1002/adhm.201701407.
[10] A. Iulian, L. Dan, T. Camelia, M. Claudia, G. Sebastian, Synthetic materials for osteochondral tissue engineering, Adv. Exp. Med. Biol. 1058 (2018) 31–52, https://doi.org/10.1007/978-3-319-76711-6_2.
[11] I. Matai, G. Kaur, A. Seyedsalehi, A. McClinton, C.T. Laurencin, Progress in 3D bioprinting technology for tissue/organ regenerative engineering, Biomaterials 226 (2020) 119536, https://doi.org/10.1016/j.biomaterials.2019.119536.
[12] B.K. Gu, D.J. Choi, S.J. Park, Y.J. Kim, C.H. Kim, 3D bioprinting technologies for tissue engineering applications, Adv. Exp. Med. Biol. 1078 (2018) 15–28, https://doi.org/10.1007/978-981-13-0950-2_2.
[13] J. Wei, F. Pan, H. Ping, K. Yang, Y. Wang, Q. Wang, Z. Fu, Bioinspired Additive Manufacturing of Hierarchical Materials: from Biostructures to Functions, vol. 6, Research (Wash D C), 2023, p. 164, https://doi.org/10.34133/research.0164.
[14] J. Zhou, C.W. See, S. Sreenivasamurthy, D. Zhu, Customized Additive Manufacturing in Bone Scaffolds-The Gateway to Precise Bone Defect Treatment, vol. 6, Research (Wash D C), 2023, p. 239, https://doi.org/10.34133/research.0239.
[15] E. Malikmammadov, T.E. Tanir, A. Kiziltay, V. Hasirci, N. Hasirci, PCL and PCL-based materials in biomedical applications, J. Biomater. Sci. Polym. Ed. 29 (7–9) (2018) 863–893, https://doi.org/10.1080/09205063.2017.1394711.
[16] S. Chae, S.S. Lee, Y.J. Choi, D.H. Hong, G. Gao, J.H. Wang, D.W. Cho, 3D cell-printing of biocompatible and functional meniscus constructs using meniscus-derived bioink, Biomaterials 267 (2021) 120466, https://doi.org/10.1016/j.biomaterials.2020.120466.
[17] V. Horbert, L. Xin, P. Föhr, R. Huber, R.H. Burgkart, R.W. Kinne, In vitro cartilage regeneration with a three-dimensional polyglycolic acid (PGA) implant in a bovine cartilage punch model, Int. J. Mol. Sci. 22 (21) (2021), https://doi.org/10.3390/ijms222111769.
[18] S. Farah, D.G. Anderson, R. Langer, Physical and mechanical properties of PLA, and their functions in widespread applications - a comprehensive review, Adv. Drug Deliv. Rev. 107 (2016) 367–392, https://doi.org/10.1016/j.addr.2016.06.012.
[19] J.K. Venkatesan, C. Falentin-Daudré, A. Leroux, V. Migonney, M. Cucchiarini, Biomaterial-guided recombinant adeno-associated virus delivery from poly(sodium styrene sulfonate)-grafted poly(ε-caprolactone) films to target human bone marrow aspirates, Tissue Eng Part A 26 (7–8) (2020) 450–459, https://doi.org/10.1089/ten.TEA.2019.0165.
[20] C.S. Moura, J.C. Silva, S. Faria, P.R. Fernandes, C.L. da Silva, J.M.S. Cabral, R. Linhardt, P.J. Bártolo, F.C. Ferreira, Chondrogenic differentiation of mesenchymal stem/stromal cells on 3D porous poly (ε-caprolactone) scaffolds: effects of material alkaline treatment and chondroitin sulfate supplementation, J. Biosci. Bioeng. 129 (6) (2020) 756–764, https://doi.org/10.1016/j.jbiosc.2020.01.004.
[21] T. Kawase, K. Yamanaka, Y. Suda, T. Kaneko, K. Okuda, H. Kogami, H. Nakayama, M. Nagata, L.F. Wolff, H. Yoshie, Collagen-coated poly(L-lactide-co-ε-caprolactone) film: a promising scaffold for cultured periosteal sheets, J. Periodontol. 81 (11) (2010) 1653–1662, https://doi.org/10.1902/jop.2010.100194.
[22] R.I. Litvinov, M. Pieters, Z. de Lange-Loots, J.W. Weisel, Fibrinogen and fibrin, in: J.R. Harris, J. Marles-Wright (Eds.), Macromolecular Protein Complexes III: Structure and Function, Springer International Publishing, Cham, 2021, pp. 471–501.
[23] J.C. Chapin, K.A. Hajjar, Fibrinolysis and the control of blood coagulation, Blood Rev. 29 (1) (2015) 17–24, https://doi.org/10.1016/j.blre.2014.09.003.
[24] T.A. Ahmed, E.V. Dare, M. Hincke, Fibrin: a versatile scaffold for tissue engineering applications, Tissue Eng Part B Rev 14 (2) (2008) 199–215, https://doi.org/10.1089/ten.teb.2007.0435.
[25] J.A. Rojas-Murillo, M.A. Simental-Mendía, N.K. Moncada-Saucedo, P. Delgado-Gonzalez, J.F. Islas, J.A. Roacho-Pérez, E.N. Garza-Treviño, Physical, mechanical, and biological properties of fibrin scaffolds for cartilage repair, Int. J. Mol. Sci. 23 (17) (2022), https://doi.org/10.3390/ijms23179879.
[26] B.A.G. de Melo, Y.A. Jodat, E.M. Cruz, J.C. Benincasa, S.R. Shin, M.A. Porcionatto, Strategies to use fibrinogen as bioink for 3D bioprinting fibrin-based soft and hard tissues, Acta Biomater. 117 (2020) 60–76, https://doi.org/10.1016/j.actbio.2020.09.024.
[27] R.I. Litvinov, J.W. Weisel, Not fibrin(ogen), but fibrinogen or fibrin, Blood 126 (17) (2015) 1977–1978, https://doi.org/10.1182/blood-2015-08-662551.
[28] Y. Zou, Z. Shan, Z. Han, J. Yang, Y. Lin, Z. Gong, L. Xie, J. Xu, R. Xie, Z. Chen, Z. Chen, Regulating Blood Clot Fibrin Films to Manipulate Biomaterial-Mediated Foreign Body Responses, vol. 6, Research (Wash D C), 2023, p. 225, https://doi.org/10.34133/research.0225.
[29] C.H. Park, K.M. Woo, Fibrin-based biomaterial applications in tissue engineering and regenerative medicine, Adv. Exp. Med. Biol. 1064 (2018) 253–261, https://doi.org/10.1007/978-981-13-0445-3_16.
[30] N. Gupta, M.A. Cruz, P. Nasser, J.D. Rosenberg, J.C. Iatridis, Fibrin-genipin hydrogel for cartilage tissue engineering in nasal reconstruction, Ann. Otol. Rhinol. Laryngol. 128 (7) (2019) 640–646, https://doi.org/10.1177/0003489419836667.
[31] K.H. Yoon, J.Y. Park, J.Y. Lee, E. Lee, J. Lee, S.G. Kim, Costal chondrocyte-derived pellet-type autologous chondrocyte implantation for treatment of articular cartilage defect, Am. J. Sports Med. 48 (5) (2020) 1236–1245, https://doi.org/10.1177/0363546520905565.
[32] S.P. Arnoczky, R.F. Warren, J.M. Spivak, Meniscal repair using an exogenous fibrin clot. An experimental study in dogs, J Bone Joint Surg Am 70 (8) (1988) 1209–1217.
[33] L.J. Reckers, D.J. Fagundes, M. Cohen, The ineffectiveness of fibrin glue and cyanoacrylate on fixation of meniscus transplants in rabbits, Knee 16 (4) (2009) 290–294, https://doi.org/10.1016/j.knee.2008.12.009.
[34] Z. Li, N. Wu, J. Cheng, M. Sun, P. Yang, F. Zhao, J. Zhang, X. Duan, X. Fu, J. Zhang, X. Hu, H. Chen, Y. Ao, Biomechanically, structurally and functionally meticulously tailored polycaprolactone/silk fibroin scaffold for meniscus regeneration, Theranostics 10 (11) (2020) 5090–5106, https://doi.org/10.7150/thno.44270.
[35] K.W. Li, T.J. Klein, K. Chawla, G.E. Nugent, W.C. Bae, R.L. Sah, In vitro physical stimulation of tissue-engineered and native cartilage, Methods Mol. Med. 100 (2004) 325–352, https://doi.org/10.1385/1-59259-810-2:325.
[36] L. Fiocco, S. Li, M.M. Stevens, E. Bernardo, J.R. Jones, Biocompatibility and bioactivity of porous polymer-derived Ca-Mg silicate ceramics, Acta Biomater. 50 (2017) 56–67, https://doi.org/10.1016/j.actbio.2016.12.043.
[37] L. Dai, Z. He, X. Zhang, X. Hu, L. Yuan, M. Qiang, J. Zhu, Z. Shao, C. Zhou, Y. Ao, One-step repair for cartilage defects in a rabbit model: a technique combining the perforated decalcified cortical-cancellous bone matrix scaffold with microfracture, Am. J. Sports Med. 42 (3) (2014) 583–591, https://doi.org/10.1177/0363546513518415.
[38] Z. Man, X. Hu, Z. Liu, H. Huang, Q. Meng, X. Zhang, L. Dai, J. Zhang, X. Fu, X. Duan, C. Zhou, Y. Ao, Transplantation of allogenic chondrocytes with chitosan hydrogel-demineralized bone matrix hybrid scaffold to repair rabbit cartilage injury, Biomaterials 108 (2016) 157–167, https://doi.org/10.1016/j.biomaterials.2016.09.002.
[39] J.H. Kellgren, J.S. Lawrence, Radiological assessment of osteo-arthrosis, Ann. Rheum. Dis. 16 (4) (1957) 494–502, https://doi.org/10.1136/ard.16.4.494.
[40] C.G. Peterfy, A. Guermazi, S. Zaim, P.F. Tirman, Y. Miaux, D. White, M. Kothari, Y. Lu, K. Fye, S. Zhao, H.K. Genant, Whole-Organ magnetic resonance imaging score (WORMS) of the knee in osteoarthritis, Osteoarthritis Cartilage 12 (3) (2004) 177–190, https://doi.org/10.1016/j.joca.2003.11.003.

[41] M. Chen, Z. Feng, W. Guo, D. Yang, S. Gao, Y. Li, S. Shen, Z. Yuan, B. Huang, Y. Zhang, M. Wang, X. Li, L. Hao, J. Peng, S. Liu, Y. Zhou, Q. Guo, PCL-MECM-Based hydrogel hybrid scaffolds and meniscal fibrochondrocytes promote Whole meniscus regeneration in a rabbit meniscectomy model, ACS Appl. Mater. Interfaces 11 (44) (2019) 41626–41639, https://doi.org/10.1021/acsami.9b13611.

[42] C. Pauli, S.P. Grogan, S. Patil, S. Otsuki, A. Hasegawa, J. Koziol, M.K. Lotz, D. D. D'Lima, Macroscopic and histopathologic analysis of human knee menisci in aging and osteoarthritis, Osteoarthritis Cartilage 19 (9) (2011) 1132–1141, https://doi.org/10.1016/j.joca.2011.05.008.

[43] J.A. van der Sluijs, R.G. Geesink, A.J. van der Linden, S.K. Bulstra, R. Kuyer, J. Drukker, The reliability of the Mankin score for osteoarthritis, J. Orthop. Res. 10 (1) (1992) 58–61, https://doi.org/10.1002/jor.1100100107.

[44] R. Kurnaz, O. Balta, Effect of platelet-rich plasma and platelet-rich fibrin matrix on healing of vertical meniscal tears in a rabbit model, Acta Orthop. Traumatol. Turcica 54 (2) (2020) 186–195, https://doi.org/10.5152/j.aott.2020.02.20.

[45] Z. Jian, T. Zhuang, T. Qinyu, P. Liqing, L. Kun, L. Xujiang, W. Diaodiao, Y. Zhen, J. Shuangpeng, S. Xiang, H. Jingxiang, L. Shuyun, H. Libo, T. Peifu, Y. Qi, G. Quanyi, 3D bioprinting of a biomimetic meniscal scaffold for application in tissue engineering, Bioact. Mater. 6 (6) (2021) 1711–1726, https://doi.org/10.1016/j.bioactmat.2020.11.027.

[46] H.J. Jeong, S.W. Lee, M.W. Hong, Y.Y. Kim, K.D. Seo, Y.S. Cho, S.J. Lee, Total meniscus reconstruction using a polymeric hybrid-scaffold: combined with 3D-printed biomimetic framework and micro-particle, Polymers 13 (12) (2021), https://doi.org/10.3390/polym13121910.

[47] Y. Zhao, K. Tan, Y. Zhou, Z. Ye, W.S. Tan, A combinatorial variation in surface chemistry and pore size of three-dimensional porous poly(ε-caprolactone) scaffolds modulates the behaviors of mesenchymal stem cells, Mater. Sci. Eng., C 59 (2016) 193–202, https://doi.org/10.1016/j.msec.2015.10.017.

[48] B.D. Smith, D.A. Grande, The current state of scaffolds for musculoskeletal regenerative applications, Nat. Rev. Rheumatol. 11 (4) (2015) 213–222, https://doi.org/10.1038/nrrheum.2015.27.

[49] W. Guo, M. Chen, Z. Wang, Y. Tian, J. Zheng, S. Gao, Y. Li, Y. Zheng, X. Li, J. Huang, W. Niu, S. Jiang, C. Hao, Z. Yuan, Y. Zhang, M. Wang, Z. Wang, J. Peng, A. Wang, Y. Wang, X. Sui, W. Xu, L. Hao, X. Zheng, S. Liu, Q. Guo, 3D-printed cell-free PCL-MECM scaffold with biomimetic micro-structure and micro-environment to enhance in situ meniscus regeneration, Bioact. Mater. 6 (10) (2021) 3620–3633, https://doi.org/10.1016/j.bioactmat.2021.02.019.

[50] S.A. Ghodbane, J.M. Patel, A. Brzezinski, T.M. Lu, C.J. Gatt, M.G. Dunn, Biomechanical characterization of a novel collagen-hyaluronan infused 3D-printed polymeric device for partial meniscus replacement, J. Biomed. Mater. Res. B Appl. Biomater. 107 (8) (2019) 2457–2465, https://doi.org/10.1002/jbm.b.34336.

[51] K.M. Fischenich, J. Lewis, K.A. Kindsfater, T.S. Bailey, T.L. Haut Donahue, Effects of degeneration on the compressive and tensile properties of human meniscus, J. Biomech. 48 (8) (2015) 1407–1411, https://doi.org/10.1016/j.jbiomech.2015.02.042.

[52] D. Deponti, A. Di Giancamillo, C. Scotti, G.M. Peretti, I. Martin, Animal models for meniscus repair and regeneration, J Tissue Eng Regen Med 9 (5) (2015) 512–527, https://doi.org/10.1002/term.1760.

[53] K.A. Athanasiou, D.J. Responte, W.E. Brown, J.C. Hu, Harnessing biomechanics to develop cartilage regeneration strategies, J. Biomech. Eng. 137 (2) (2015) 020901, https://doi.org/10.1115/1.4028825.

[54] Y. Li, H. Meng, Y. Liu, B.P. Lee, Fibrin gel as an injectable biodegradable scaffold and cell carrier for tissue engineering, ScientificWorldJournal 2015. http://doi.org/10.1155/2015/685690, 2015.

[55] T. Rasheed, M. Bilal, Y. Zhao, A. Raza, S.Z.H. Shah, H.M.N. Iqbal, Physiochemical characteristics and bone/cartilage tissue engineering potentialities of protein-based macromolecules - a review, Int. J. Biol. Macromol. 121 (2019) 13–22, https://doi.org/10.1016/j.ijbiomac.2018.10.009.

[56] Z.H. Wang, X.J. He, Z.Q. Yang, J.B. Tu, Cartilage tissue engineering with demineralized bone matrix gelatin and fibrin glue hybrid scaffold: an in vitro study, Artif. Organs 34 (2) (2010) 161–166, https://doi.org/10.1111/j.1525-1594.2009.00856.x.

[57] J.M. Anderson, Inflammatory response to implants, ASAIO (Am. Soc. Artif. Intern. Organs) Trans. 34 (2) (1988) 101–107, https://doi.org/10.1097/00002480-198804000-00005.

[58] D.N. Maianskiĭ, [Problems of Chronic Inflammation in Current Pathophysiology], Patol Fiziol Eksp Ter (2), 1994, pp. 51–55.

[59] R. Medzhitov, Origin and physiological roles of inflammation, Nature 454 (7203) (2008) 428–435, https://doi.org/10.1038/nature07201.

[60] J. Li, J. Chen, R. Kirsner, Pathophysiology of acute wound healing, Clin. Dermatol. 25 (1) (2007) 9–18, https://doi.org/10.1016/j.clindermatol.2006.09.007.

[61] L. Zhao, X. Li, L. Yang, L. Sun, S. Mu, H. Zong, Q. Li, F. Wang, S. Song, C. Yang, C. Zhao, H. Chen, R. Zhang, S. Wang, Y. Dong, Q. Zhang, Evaluation of remodeling and regeneration of electrospun PCL/fibrin vascular grafts in vivo, Mater. Sci. Eng., C 118 (2021) 111441, https://doi.org/10.1016/j.msec.2020.111441.

[62] S. Freeman, R. Ramos, P. Alexis Chando, L. Zhou, K. Reeser, S. Jin, P. Soman, K. Ye, A bioink blend for rotary 3D bioprinting tissue engineered small-diameter vascular constructs, Acta Biomater. 95 (2019) 152–164, https://doi.org/10.1016/j.actbio.2019.06.052.

[63] E.H. Backes, S.V. Harb, C.A.G. Beatrice, K.M.B. Shimomura, F.R. Passador, L. C. Costa, L.A. Pessan, Polycaprolactone usage in additive manufacturing strategies for tissue engineering applications: a review, J. Biomed. Mater. Res. B Appl. Biomater. 110 (6) (2022) 1479–1503, https://doi.org/10.1002/jbm.b.34997.

[64] J.A. Kim, Y.H. An, H.G. Yim, W.J. Han, Y.B. Park, H.J. Park, M.Y. Kim, J. Jang, R. H. Koh, S.H. Kim, N.S. Hwang, C.W. Ha, Injectable fibrin/polyethylene oxide semi-IPN hydrogel for a segmental meniscal defect regeneration, Am. J. Sports Med. 49 (6) (2021) 1538–1550, https://doi.org/10.1177/0363546521998021.

[65] M.D.M. Lombardo, L. Mangiavini, G.M. Peretti, Biomaterials and meniscal lesions: current concepts and future perspective, Pharmaceutics 13 (11) (2021), https://doi.org/10.3390/pharmaceutics13111886.

[66] A.R. Merriam, J.M. Patel, B.M. Culp, C.J. Gatt Jr., M.G. Dunn, Successful total meniscus reconstruction using a novel fiber-reinforced scaffold: a 16- and 32-week study in an ovine model, Am. J. Sports Med. 43 (10) (2015) 2528–2537, https://doi.org/10.1177/0363546515595065.

[67] J.M. Patel, A.R. Merriam, B.M. Culp, C.J. Gatt Jr., M.G. Dunn, One-Year outcomes of total meniscus reconstruction using a novel fiber-reinforced scaffold in an ovine model, Am. J. Sports Med. 44 (4) (2016) 898–907, https://doi.org/10.1177/0363546515624913.